Chapter 3

Experimental and characterization techniques

§ 3.1 Initial synthesis methods

§ 3.1.1 Liquid-Phase Pulsed Laser Ablation

In this study, various nanostructured materials were prepared by liquid-phase pulsed laser ablation (Chapter 2). The experimental parameters and schematic diagram of the LP-PLA system [1] are shown in Table 3.1 and Figure 3.1, respectively. A solid target was ablated at room temperature while submerged in a 5 ml solution inside a sealed stainless steel cell. In order to reduce the effect of target aging, the cell was rotated at 700 r.p.m. during ablation using a standard magnetic stirrer. A Q-switched Nd:YAG laser (532 nm, pulse duration 15 ns, frequency 10 Hz) was directed by a prism and then focused onto the solid target surface using a 25 mm-focal-length lens. The intense laser light passed through a quartz window in the top of the cell, then through ~5 mm layer of the liquid covering solid target, to form a ~0.5 mm-diameter spot on the target surface. This resulted in high energy density at the target and subsequently it caused vaporization and ablation of target material as a plasma plume. Ablated material was then held in suspension, in the liquid phase, removed and then stored in air-tight vials for analysis.

The apparatus (as shown in Figure 3.2) was enclosed within a light-tight box to prevent laser light reflecting into the laboratory. All of the components are bolted to a laser bench. The height of the lens is controlled by a micrometer, which enables the precise focusing necessary with a short focal length lens. The target cell is on a

horizontal translation stage and that allows the laser to be focused on selected areas of the target. An extractor fan was added to remove fumes from the liquid phase, in particular those from ammonia solution.

Table 3.1 Experimental parameters used during LP-PLA process

Excimer laser power (Nd:YAG 532 nm)	25-125 mJ
Focus lens	f = 25 mm
Solid target	Graphite (Testbourne Ltd., 99.99%) Zn plate (Fisher Scientific, 99.99%)
Liquid solution	1) 25%-35% Ammonia solution (Fisher Scientific, used as received without further purification) 2) Aqueous solution with various concentration of surfactant SDS 3) deionised water 4) Cyclohexane 5) Toluene 6) Benzene 7) Hexane
Ablation time (t)	10 min-24 h

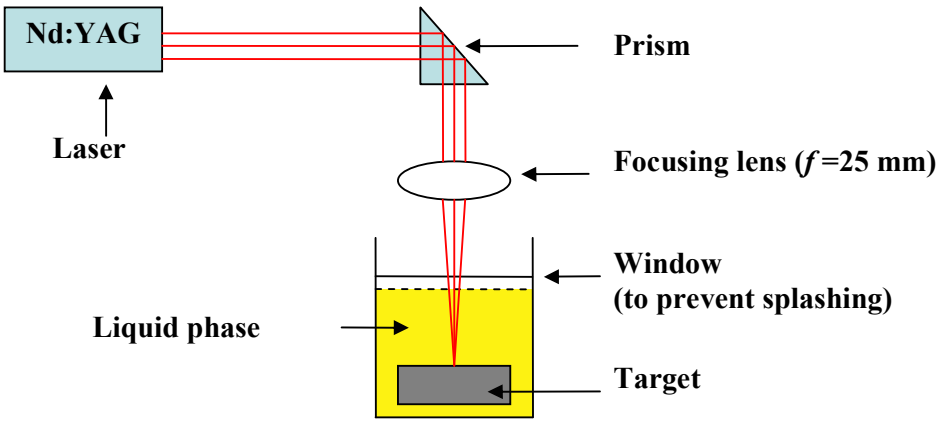

Figure 3.1 Schematic diagram of the basic LP-PLA system used in these studies.

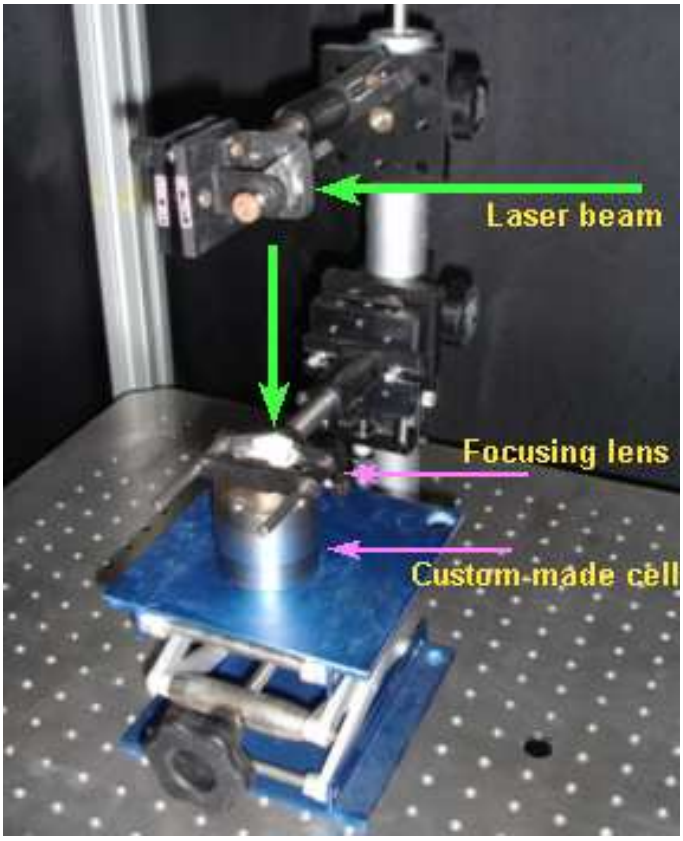

Figure 3.2 Experimental apparatus setup.

§ 3.1.2 Nd:YAG laser

Nd:YAG (neodymium-doped yttrium aluminium garnet, Nd:$Y_3Al_5O_{12}$) is a crystal that is used as a lasing medium for solid-state lasers. The dopant, triply ionized neodymium, typically replaces yttrium in the crystal structure, since they are of similar size. Generally, the crystalline host is doped with around 1% neodymium by weight. Laser operation of Nd:YAG was first demonstrated by Geusic *et al.* at Bell laboratories in 1964 [2].

Nd:YAG lasers typically emit light with a wavelength of 1064 nm, in the infrared. However, there are also transitions near 940, 1120, 1320 and 1440 nm. Nd:YAG lasers operate in both pulsed and continuous mode. Pulsed Nd:YAG lasers are typically operated in the so called Q-switching mode: An optical switch is

inserted in the laser cavity waiting for a maximum population inversion in the neodymium ions before it opens. Then the light wave can traverse the cavity, depopulating the excited laser medium at maximum population inversion. In this Q-switched mode, output powers of 20 MW and pulse durations of less than 10 ns are achieved.

The laser used in this work is a Spectron laser system Class IV (Figure 3.3), which provides laser output at 532 nm. This allowed easier and safer directing and focusing of the beam onto the target. The laser had a pulse length of 15 ns and a maximum output of 175mJ / pulse.

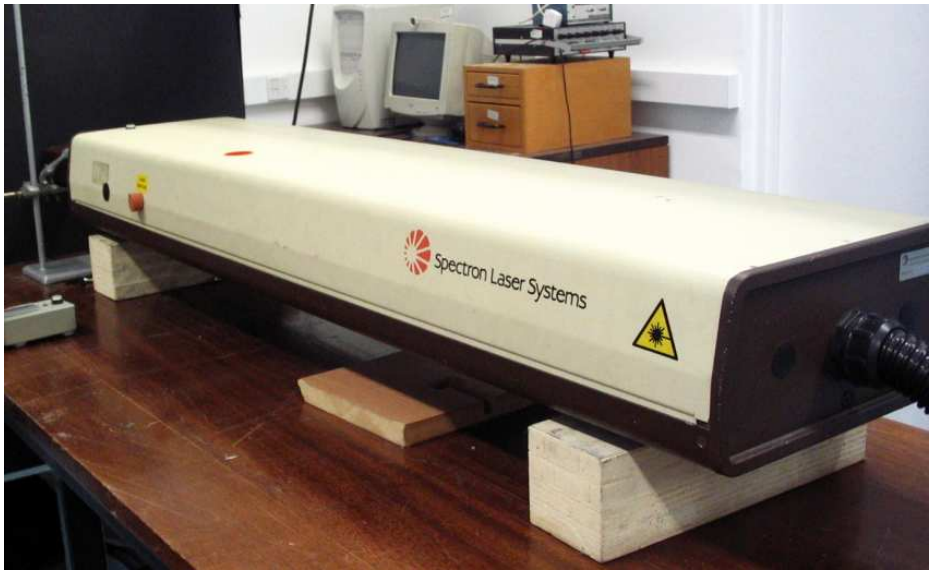

Figure 3.3 Photograph of the Nd:YAG laser used in this study.

§ 3.1.3 The Reaction Cell

There were two types of reaction cell used during the laser ablation. The first type of cell was a simple open container, which allowed the ablation plume to be viewed easily for optical emission experiments. However, this cell had the disadvantage that the liquid could splash out from the cell at every laser pulse, requiring the liquid level to be constantly topped-up. That means the experiment had

to be stopped on several occasions during an ablation run to refill the liquid. If the lens or prism were splashed, the laser did not focus properly on the target surface and the power density was reduced. As a result, the experiment sometimes needed to be stopped temporarily while the optics were wiped clean. Moreover, the depth of the liquid in the open cell gradually drops, and most of the product was lost due to the splashing. This made control of the experimental conditions difficult. Therefore, target cell modifications were required.

The second type of cell was a special custom-made sealed stainless steel cell, which prevented the splashing but had less access for spectroscopic measurements. This cell was made up of three sections strongly bolted together (Figure 3.4). This allowed the size of the middle section to be varied, and therefore also the liquid phase level. The cell can withstand the high pressures that could be produced when the laser power is deposited inside the closed structure. A glass window was placed on the top of the cell to prevent splashing of the liquid phase and hence loss of ablated materials. Unless mentioned specifically (*e.g.* in Appendix A), the experiments in this thesis were carried out in the sealed cell.

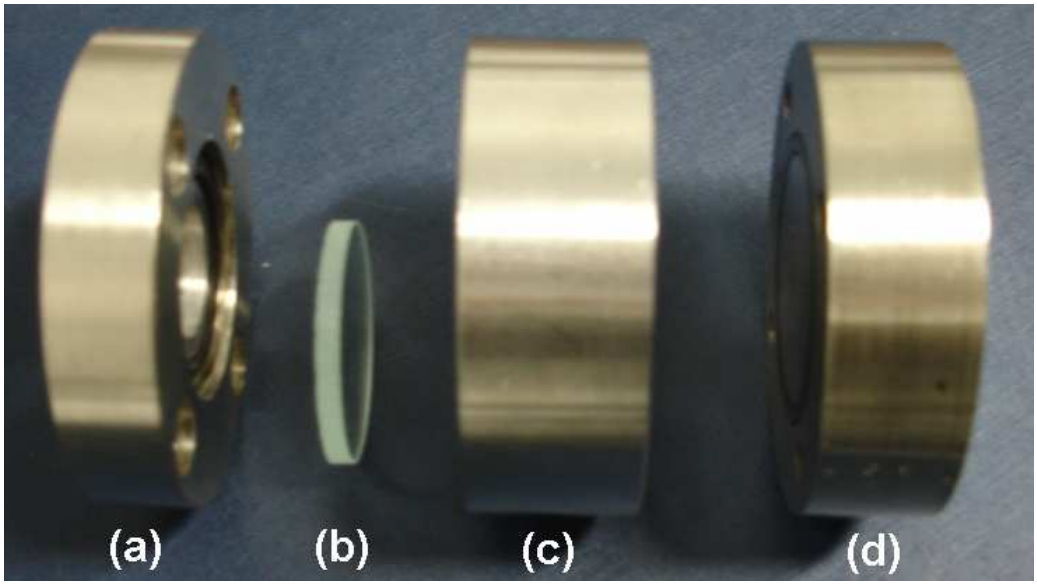

Figure 3.4 Custom-made stainless steel cell (a) top with indent and O-rings to hold the glass window, (b) glass window, (c) middle section, variable in width and with a 16 mm-diameter hole throughout, (d) base. The sections are bolted together.

§ 3.1.4 Ablation procedure

A graphite rod with a diameter of 16 mm was bought from Testbourne Ltd to use as a target, which fits the sealed cell exactly. The cell is also the same size as the die used in the hydraulic press to produce pellets from the powder. The middle section and base can be bolted together so that a target can be pressed directly into the cell. Hence, the modified cell design allowed systematic investigation of different target compositions.

The liquid medium (*e.g.* water, ammonia solution, *etc*) was added to the cell and filled to the top of the glass window, with no air gap. This is necessary to prevent the droplets or bubbles appearing underneath the window during laser ablation. When assembling the cell, great care was taken not to introduce any bubbles into the system, since these would rise to the underside of the window and prevent the laser from focusing properly on the target surface. The cell was then placed into the path of the laser beam.

The laser beam was focused down to the smallest spot possible, by using the single-shot mode. This was done either by moving the lens up and down or by moving the reaction cell up and down using a lab jack. It is estimated that the energy density at the target had a maximum fluence of 15 J cm^{-2} from a laser spot size approximately 0.5 mm in diameter.

When the laser fired, a loud cracking noise was heard from the reaction cell as the ablation process occurred. The volume of the sound can be reduced significantly if the laser alignment was carried out as accurately as possible. Light emission from the plume above the focal point was also observed, and recorded using Optical Emission Spectroscopy (OES). In some cases, a small area of the window turned white and fine cracks occurred due to laser damage. With this weak spot in the glass, the pressure within the cell caused the whole window to crack. To prevent this problem, a short focal length lens (25 mm) was used so that the power density at the window was not sufficient to cause damage while still achieving a precise focus at the target surface.

§ 3.1.5 Sample separation and further analysis preparation

When ablating the graphite target (for other targets used please see the corresponding chapter), a pale colour colloidal suspension was obtained depending on the target and liquid used, which contained a mixture of unreacted target materials and ablation product, both in the form of nanoparticles (NPs). The suspension was repeatedly centrifuged at 13000 rpm, and the liquid decanted off. The solid sediment was washed several times with deionised water and dried overnight at 60˚C in an oven, before further characterization. In order to remove as much of the unwanted graphitic impurities from the product as possible, the sediment was boiled in 70% perchloric acid (Fisher Scientific, used as received without further purification) for 60 mins, and then filtered.

A suspension of the purified product in water was pipetted onto a carbon-coated transmission electron microscopy (TEM) grid or a SiO_2-coated grid (Agar Scientific) to ensure that the elemental fingerprint of the sample was not confused with that from the grid, washed several times (using deionised water) in order to remove liquid solution traces, and then allowed to dry in air. For analysis by X-ray diffraction (XRD), X-ray photoelectron spectroscopy (XPS) and Laser Raman Spectroscopy (LRS) the concentration of ablation products in the suspension needed to be increased by evaporation of some of the liquid phase in an oven. This concentrated suspension was then pipetted onto a glass slide and dried to produce a thin layer. This pipetting and drying procedure was repeated many times to increase the thickness of the layer sufficient to obtain a high signal:noise ratio in the subsequent analysis.

§ 3.2 Sequential deposition and self-assembly

§ 3.2.1 General two-step deposition

The fabrication of well-defined two-dimensional (2D) and three-dimensional (3D) nanostructures is usually difficult because control of the nucleation and growth

is still a challenge. Complex architectures are normally related to multi-step syntheses, which begin with substrate surface preparation for heterogeneous nucleation of oriented nanocrystals. Two basic approaches have been used: one is deposition on chemically modified interfaces using organic self-assembled monolayers (SAMs) [3]. Another, more straightforward method, is to seed the substrate with NPs of the desired film material [4]. The fundamental advantage of seeded growth is enhanced control, obtained by separating the NP film nucleation and oriented rod growth into two steps. The possibility of forming increasingly complex structures by seeding control, such as multi-level branched structures, opens the door to more complex three-dimensional materials and devices exploiting the unique properties of nanomaterials. Recently, Dick *et al*. [5] and others have used secondary seeding of Au nanoclusters on III-V nanowires in order to produce branched and hyperbranched structures. The authors demonstrated that the diameter, length, number, and chemical composition of each branch can be controlled. Such control of three-dimensional networked structures suggests great potential for even larger structures and their utilization in nanoscale devices and systems.

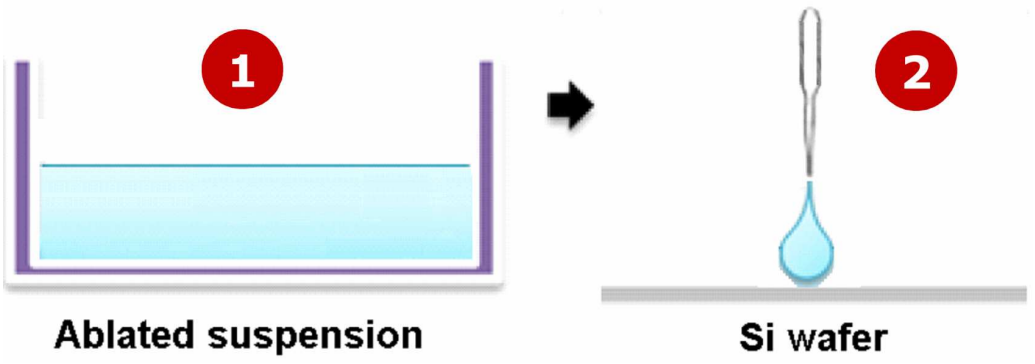

Figure 3.5 Schematic diagram of a two-step strategy for increasing the complexity of the nanostructures.

To date, most nanomaterials made by LP-PLA have been either continuous film structures, zero-dimensional (0D) NPs, or one-dimensional (1D) nanorods (NRs). Since the 0D and 1D nanocrystals can serve as building blocks in forming 2D or 3D

complex architectures with long term periodic structures, it should be expected that the LP-PLA approach would have great potential as a means to grow large arrays of hierarchical, complex, oriented and ordered superstructures. Extending this concept, we performed a two-step synthesis to produce oriented carbon nitride nanostructures. Many more complex nanostructures than simple NPs and NRs can be produced in a controlled fashion by simply altering the drying time and drying method of the suspension of ablated product. In this methodology, the carbon nitride materials produced in the initial LP-PLA step were physically deposited onto a silicon p-(100) substrate. The liquid was then removed by drying. Aerosol NPs offer great advantage in this case, as they are easily deposited onto complex structures and are known to govern accurately the diameter of the nanowires for which they are the seeds [6,7]. This new combination of technologies represents a significant step in the pursuit of functional nanoscale devices and nanomaterials, as the multi-step procedure allows a level of control and flexibility not previously seen.

§ 3.2.2 Main drying process

Four different drying processes were used in the present study: (1) dry naturally in air; (2) dry in a sealed tube; (3) dry in an oven or on a hotplate; (4) dry in a critical point dryer (CPD). Those procedures allowed the time taken to evaporate the liquid to be controlled.

CPD is a widely used drying technique in which the surface tension can be reduced to zero during evaporation [8]. The air (evaporative) drying of specimens can cause deformation and collapse of structures, the primary cause of such damage being the effects of surface tension. The specimen is subjected to forces, which are present at the phase boundary, as the liquid evaporates. The most common specimen medium, water, has a high surface tension to air; by comparison that for acetone is several times lower. The surface tension could be reduced by substitution of a liquid with a lower surface tension with expectations of reduced damage during air-drying. Critical Point Drying includes the occurrence known as the 'continuity of state' for which there is no apparent difference between the liquid and gas state of a medium, the surface tension between this interface reducing to zero. This occurs at a specific

temperature and pressure with resulting density, and is known as the Critical Point. When this 'critical point' is reached, it is possible to pass from liquid to gas without any abrupt change in state.

The Emitech K850 Critical Point Drier was used in our study. CPD is designed for use with liquid CO_2, having first replaced any water in the specimen by a series of dehydration with the help of acetone. The specimens for CPD were placed into the pressure chamber. The chamber was vertical, with top loading, to ensure specimens did not become uncovered during the drying process, with a side viewing port to locate the miniscus for the correct level when initially filling the chamber. The chamber was pre-cooled to 5ºC allow it to be readily filled with liquid CO_2 from a gas cylinder. The chamber was then heated to just above the critical temperature (35ºC) with subsequent critical pressure (1350 p.s.i.) being achieved. The CO_2 gas was vented through a needle valve, to avoid specimen distortion. The whole procedure normally took about 45 min.

§ 3.3 Materials analysis methods

§ 3.3.1 Micro-Combustion Elemental Analysis

Micro-combustion elemental analysis is a relatively simple method of determining the composition of organic materials. Elements detectable by these methods include carbon, hydrogen, nitrogen, the halogens, sulfur and oxygen [9].

Samples were packed into an oxidisable container and then dropped into a heated quartz tube, through which a constant flow of helium was passed. As the sample was introduced, oxygen was added to the helium stream causing combustion of the sample. All carbon, hydrogen and nitrogen in the sample were converted to CO_2, H_2O and NO_x during the flash combustion. The inert flow of helium carried these compounds over heated copper, reducing the NO_x to N_2. The gases were then separated by a gas chromatograph and detected by thermal conductivity measurements [10].

In this study, micro-combustion elemental analysis to identify carbon nitride (about 5 mg sample) formation was performed by Des Davis in the Macromolecular Lab at the School of Chemistry, University of Bristol.

§ 3.3.2 X-ray Powder Diffraction (XRD)

X-ray diffraction (XRD) is one of the primary techniques used by mineralogists and solid state chemists for the characterisation of crystalline solids and determination of their structure. About 95% of all solid materials can be described as crystalline and when X-rays interact with a crystalline phase, a diffraction pattern is generated as a result of the interaction between the incident X-rays and the atomic architecture of the solid.

Each crystalline solid has unique atomic architecture and consequently has a unique characteristic X-ray powder pattern. These patterns can be used as 'fingerprints' for identification of solid phases. Once the material has been identified, X-ray crystallography may be used to determine its structure, *i.e*. how the atoms pack together in the crystalline state and the size and the shape of the unit cell, *etc*.

When X-rays interact with atoms in two lattice planes, and the path length difference between rays equals a whole multiple of the wavelength of the radiation, constructive interference occurs (Figure 3.6). Bragg's law describes the conditions for constructive interference in certain directions and the production of diffracted scattered X-rays:

$$n\lambda = 2d \sin\theta \qquad (3.1)$$

Where n = an integer,

λ = the wavelength of the X-rays

d = the spacing between 2 atom layers

θ = the angle between the incoming X-ray and the atom layer.

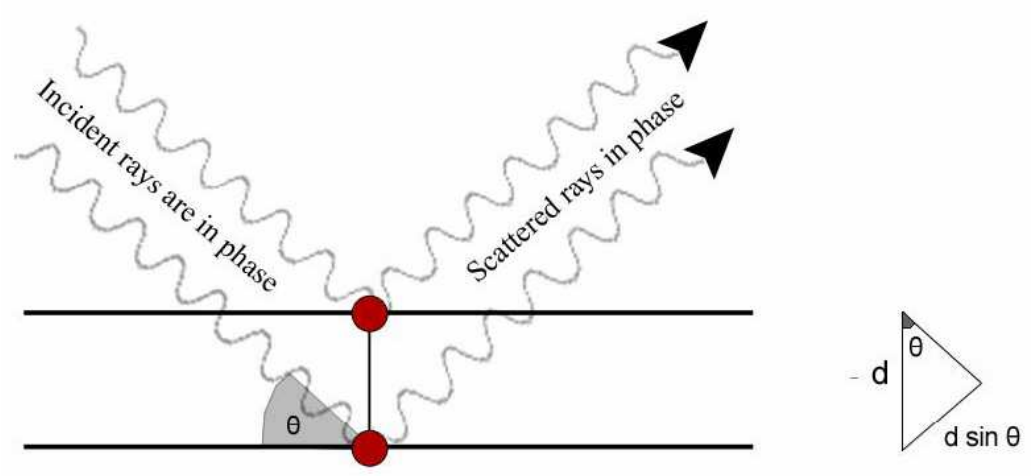

Figure 3.6 An X-ray diffraction beam schematic [11], showing the incident and scattered X-rays, from a pair of atoms in different lattice planes. The relation by which diffraction occurs is known as Bragg's law.

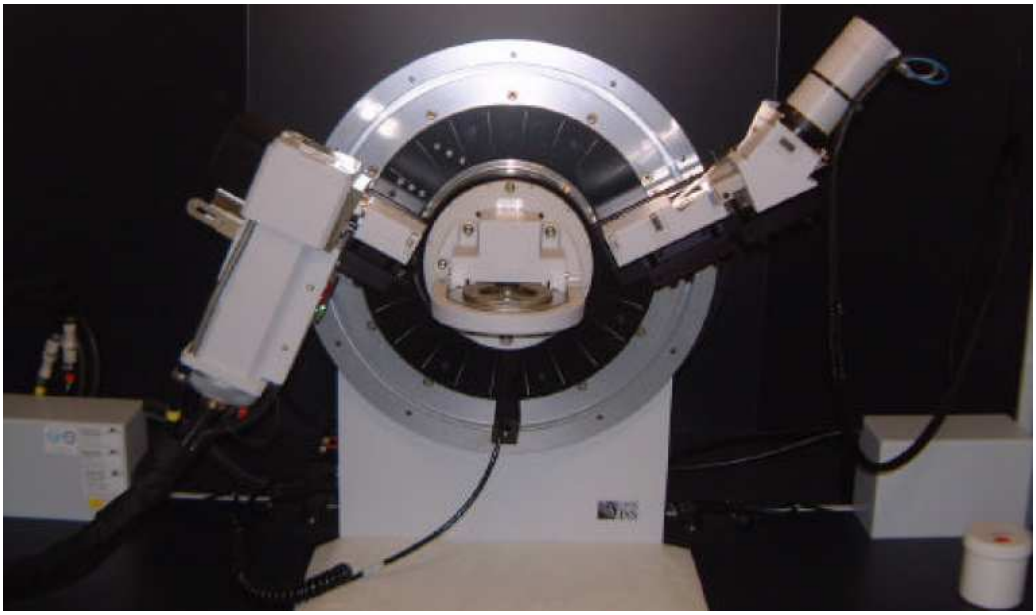

Figure 3.7 Photograph of the X-ray powder diffractometer used in this study, the X-ray source is on the left, the sample is in the middle and the detector is on the right.

This is the basic relationship among the spacing between the lattice planes (*d*-spacing), the wavelength and the angle (θ) of observation in a diffraction experiment. The angle between the incident and diffracted beams is 2θ degrees.

The XRD equipment used in this study was a Bruker-Nonius D8 Powder Diffractometer (Figure 3.7). The wavelength of the X-ray source employed is 1.54056 Å (Copper Kα) with a photon energy of 8 keV.

§ 3.3.3 Scanning Electron Microscopy (SEM)

Electron microscopes were developed in the 1930s to overcome the limitations of optical microscopy and provide increased magnification and resolution, far superior to optical systems. The first commercialized SEM was built by Cambridge Instruments. For detailed history of the SEM's development, see Goldstein [12].

SEM is a powerful tool for examining and interpreting microstructures of materials, and is widely used in the field of material science. The principle of SEM is based on the interaction of an incident electron beam and the solid specimen [13]. Electron bombardment can produce a wide variety of emissions from the specimen, including backscattered electrons, secondary electrons, Auger electrons, X-rays, visible photons and so on.

1) **Secondary Electrons**: If an incident electron collides with an electron in a sample atom, it will knock the electron out of its orbital shell and the atom will become ionised. Because the incident electron loses little energy during each collision, multiple collisions are possible, continuing until the incident electron no longer has the energy to dislodge secondary electrons. Each freed secondary electron has a very small kinetic energy (<50 eV), which is independent of the incident electron energy. If generated close enough to the sample surface (<10 nm), these secondary electrons can escape to be collected by the detector. As a direct result, secondary electron imaging is closely related to sample topography.
2) **Backscattered Electrons**: If an incident electron collides with the nucleus of surface atom, the electron will bounce or scatter 'backward' out of the sample as

a backscattered electron (BSE). These electrons have high energies, typically between 50 eV and that of the original incident electron. The production of backscattered electrons varies directly with atomic number, and thus backscattered electron images can be used to discern differences in sample atomic number.

3) **Auger Electrons**: As a result of secondary electron generation, a vacancy is left in an ionised atom's electron shell. To fill this vacancy, an electron from a higher energy outer shell (from the same atom) can drop down to fill the vacancy. This creates an energy surplus in the atom that can be corrected by emitting an outer electron, an Auger electron. Auger electrons have a characteristic energy unique to the element from which they are emitted and can be used to give compositional information about the target sample. Auger electrons have a relatively low kinetic energy and are only emitted from shallow sample depths (<3 nm).
4) **Characteristic X-rays***:* X-rays are also produced by interactions of the incident electron beam with a sample surface. Similar to the Auger electron generating process, the excess energy produced by reshuffling electrons to fill shell vacancies can also be emitted in the form of an X-ray rather than an Auger electron. X-rays have a characteristic energy unique to the element from which they originate and so provide compositional information about a sample.

Secondary electron imaging and X-ray analysis were the primary functions used for SEM sample characterisation in this study.

An SEM consists of three distinct parts: an electron column; a detection system; and a viewing system. Figure 3.8 shows a schematic of a simple scanning electron microscope. Two electron beams are controlled simultaneously by the same scan generator: one is the incident electron beam; the other is for the cathode ray tube (CRT) screen. The incident beam is scanned across the sample, line by line, and the signal from the resulting secondary electrons is collected, detected, amplified and used to control the intensity of the second electron beam. Thus a map of intensity of secondary electron emission from the scanned area of the sample will be shown on the CRT screen as variations in brightness, reflecting the surface morphologies of the

specimen. Given this mechanism, the magnification of the SEM image can be adjusted simply by changing the dimensions of the area scanned on the sample surface.

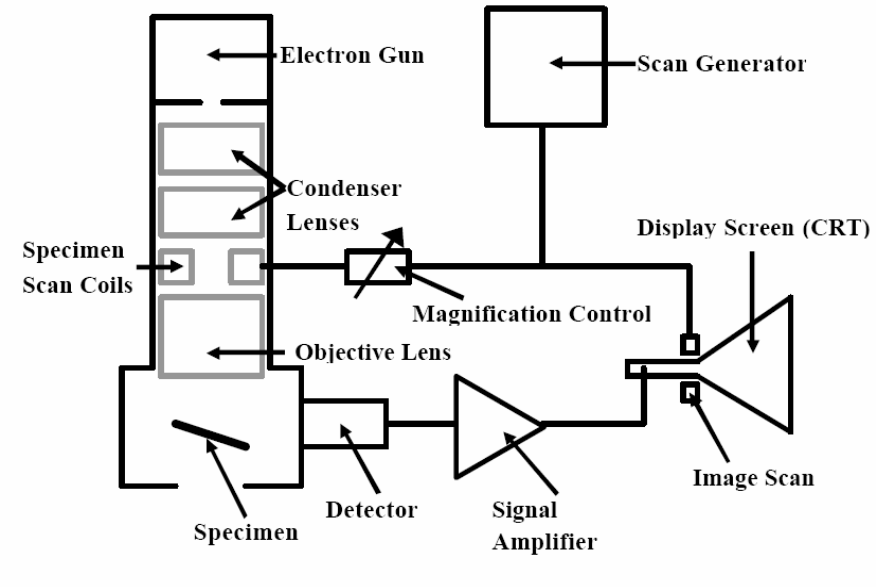

Figure 3.8 Schematic diagram of a scanning electron microscope.

Figure 3.9 A photo of FESEM JEOL 6300 FEG microscope in University of Bristol. (http://www.chm.bris.ac.uk/emuweb/6300f.htm)

The spatial resolution of the SEM is strongly dependent on diameter (spot size) of the electron probe beam at the specimen surface. In a SEM system, the diameter of the incident electron beam is demagnified using two or more electron lenses before it reaches the sample surface. At the same time, the effective diameter of the electron source is a key factor in determining the resolution of the SEM. There are two basic types of electron guns in current use: thermionic electron gun and field emission electron gun. The diameters of the electron beam originating from these gun types are about 20-50 μm and 10 nm, respectively. Thus, field emission SEM (FESEM) is the electron source of choice for high-resolution SEM images.

The SEM systems employed in this work are a JEOL SEM 5600 LV and a JEOL FESEM 6330 FEG. Figure 3.9 shows a photo of the JEOL FESEM 6330 FEG using in Bristol. Sample used for SEM observation were sputtered with ~15 nm platinum to reduce the changing effect.

§ 3.3.4 Transmission Electron Microscopy (TEM) and High Resolution (HR) TEM

TEM is one of most powerful techniques in materials science, which has been widely used in the characterization of nanocomposites. It has ability to examine the constitutional characteristics of these nanocomposites such as grain shape and size, crystallinity and chemical variations at a resolution down to the nanometer scale. With advanced design, modern TEM enables lattice defects, atoms and even their movements to be seen.

The first practical TEM was built by Albert Prebus and James Hillier at the University of Toronto in 1938 using concepts developed earlier by Max Knoll and Ernest Ruska [14]. Since then, the TEM has had considerable development and is now becoming a versatile tool of characterization in material science and biology. In terms of its construction (a schematic diagram shown in Figure 3.10), a general TEM usually consists of six basic components, as follows:

1) **Source providing illumination**: An electron source, commonly used in all TEM, comprises a filament, which emits electrons either by thermal heating (a so-called

thermionic filament) or through application of high electric field to a metal filament tip generating field emission electrons (so-called field-emission filament). The field-emission filament is a lot more expensive and requires much higher vacuum than the thermionic filament, but offers a very stable source with a greater resolution and longer life-time.

2) **Electrodes**: These include a cathode, which accelerates the electrons generated from the filament to a high energy, ranging from a few hundreds to over million volts. Although a higher voltage can produce a higher resolution, in fact, most TEM instruments are operated at energies between 100 kV and 400 kV. This is to reduce sample damage and the cost of the instrument while still achieving an electron wavelength as short as possible.

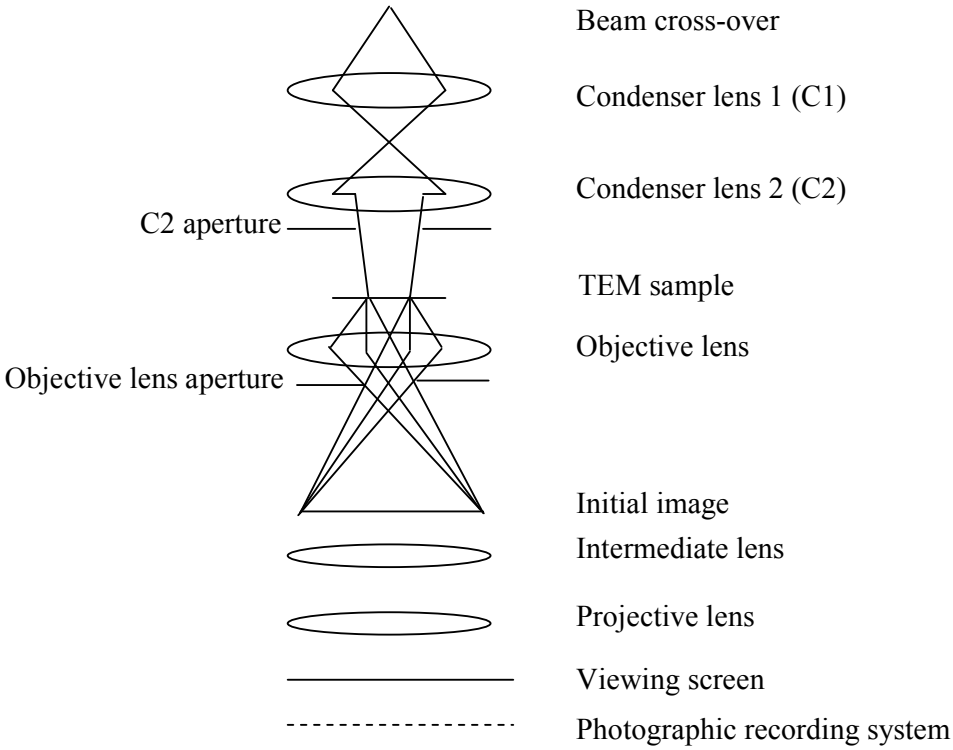

Figure 3.10 Schematic diagram of transmission electron microscope

3) **An optical system**: This consists of a series of electromagnetic lenses, such as condenser lens, objective lens, projective lens as well as intermediate lens. These lenses help to focus the electrons to produce a small probe beam and form images of samples. The objective lens is the heart of the microscope. The spherical and chromatic aberrations inherent in the objective lens are the major limitations to the resolution of the TEM instrument.
4) **A sample chamber**: This is where the sample is positioned, and is directly above the objective lens. It is important that the chamber is spacious enough to allow the samples to be viewed with a wide range of tilting necessary for the crystal orientation examination as well as for chemical analysis.
5) **Camera(s)**: Images of the samples can be acquired using a video/scanned camera which is located beneath a phosphor screen where the images are seen. The photographs are taken by lifting up the screen and exposing the film in the camera. However, this recording method has been gradually replaced by using a charge-coupled device (CCD) camera, which collects a digital image which can be saved onto a computer.
6) **Vacuum system**: The TEM runs at a very high vacuum, which is maintained by a vacuum system. In most cases, such a system comprises a combination of two types of pumps, *i.e.* mechanical and diffusion pumps.

The analysis capacity of TEM has been significantly enhanced by integration of several advanced techniques into the instrument. These techniques include spectrometers, such as energy-dispersive X-ray analysis (EDX) and electron energy-loss spectroscopy (EELS).

Nowadays, there is increasing demand to produce an image at an atomic scale so that the lattice arrangements within crystalline materials can be visualized. One well-known technique for this is high resolution TEM (HRTEM). A very high magnification is necessary in order to obtain a high-resolution atomic image. However, such an atomic image is not turned out by simply zooming into an image to a sufficient magnification through an imaging system (comprising of both intermediate and projection lenses) in TEM. As a result, quite a few things must be taken into account in order to acquire a good quality HRTEM image. First, TEM

column alignment needs to be carried out as accurately as possible, which includes electron gun and condenser lens alignment, plus astigmatism correction of condenser lenses and objective lens. Secondly, in a HRTEM, an atomic image of a crystal structure is only possible if certain conditions are satisfied, one of which - choosing the optimum defocus - is crucial.

To examine materials by TEM requires a sample that normally should be less than 3 mm in diameter with the area of interest sufficiently thin to allow electrons to penetrate it. It is very important to prepare a good TEM sample, which is a prerequisite for any analysis using various TEM techniques (including imaging, EDX and others). Not only is it difficult to thin the bulk sample down to the desired thickness (mostly less than 100 nm), but also preparation (such as mechanical/electrochemical polishing and ion sputtering) can create a lot of artifacts in and on the sample, which may give rise to false information.

Figure 3.11 A photo of the TEM JEOL 2010 microscope in the University of Bristol. (http://www.chm.bris.ac.uk/emuweb/2010.htm).

The TEMs used in present study were a JEOL 1200 with a 120 kV electron source, a JEOL 2100 with a 200 kV electron source and a JEOL 3000 F with a 300 kV (hosted in the University of Oxford). A photo of the JEOL 2010 microscope is shown in Figure 3.11.

§ 3.3.5 Selected Area Electron Diffraction (SAED) and Microdiffraction Pattern (MDP)

Selected area electron diffraction (SAED) is a crystallographic experimental technique that can be performed inside a TEM to identify crystal structures and examine crystal defects [15]. It is similar to X-ray diffraction, but unique in that areas as small as several hundred nm in size can be examined, whereas X-ray diffraction typically samples areas several cm in size. SAED is used primarily in material science and solid state physics, and is one of the most commonly used experimental techniques in those fields.

In a TEM, a thin crystalline specimen is subjected to a parallel beam of high-energy electrons. As TEM specimens are typically ~100 nm thick, and the electrons typically have an energy of 100-400 kV, the electrons pass through the sample easily. Some fraction of them will be scattered to particular angles, determined by the crystal structure of the sample, while others continue to pass through the sample without deflection. By inserting a selected area aperture strip, located below the sample holder on the TEM column, all of the electron beam will be blocked except for the small fraction passing through to contribute to a diffraction pattern on the screen. The resulting diffraction pattern is then recorded on photographic film or using a CCD camera.

In relation to diffraction patterns, there are three types of solid matter: single crystals, polycrystals and amorphous materials.

(i) **Single crystals** consist of atoms arranged in an ordered lattice. An electron beam passing through a single crystal will produce a pattern of spots (see Figure 3.12(a)). From the diffraction spots one can determine the type of crystal structure (f.c.c., b.c.c.) and the 'lattice parameter' (*i.e.*, the distance

between adjacent (100) planes). Also, the orientation of the single crystal can be determined: if the single crystal is turned or flipped, the spot diffraction pattern will rotate around the centre beam spot in a predictable way.

(ii) **Polycrystalline materials** are made up of many tiny single crystals. Any small single crystal in a polycrystal will have a random distribution of all the possible orientations. A polycrystal, therefore, will produce a diffraction pattern equivalent to that produced by a beam passing through series of single crystals of various orientations. A series of concentric rings are formed, resulting from many spots very close together at various rotations around the centre beam spot. Each circle corresponds to a different set of Miller indices. From the diffraction rings one can also determine the type of crystal structure and the 'lattice parameter'. However, the determination of the orientation of a polycrystal is not possible since there is no change for the ring pattern when flipping or turning the polycrystal.

(iii) **Amorphous materials** do not consist of atoms arranged in ordered lattices, but in random sites. Therefore, amorphous materials are completely disordered. The electron diffraction pattern will consist of fuzzy rings of light on the fluorescent screen.

The geometry of an electron diffraction experiment is shown in Figure 3.12(b). By indexing the diffraction pattern, a major phase in the nanomaterial can be identified using the following equations:

The Bragg law for small angles approximates to: $\lambda = 2d\theta$ (3.2)

From the diagram: $\frac{R}{L} = 2\theta$ (3.3)

Therefore: $\frac{R}{L} = \frac{\lambda}{d}$ or $L\lambda = Rd$ (3.4)

where L is the TEM camera length used to record the image. Often the value of $L\lambda$ is referred to as the 'camera constant' of the microscope. R refers to the radius of each ring or the distance of a diffraction spot from the direct beam spot on the diffraction pattern, and d represents the lattice constant of the phase. The working distances L of the TEM JEOL 1200 and HRTEM JEOL 2010 microscope used in the present work were fixed to 100 cm and 120 cm, respectively.

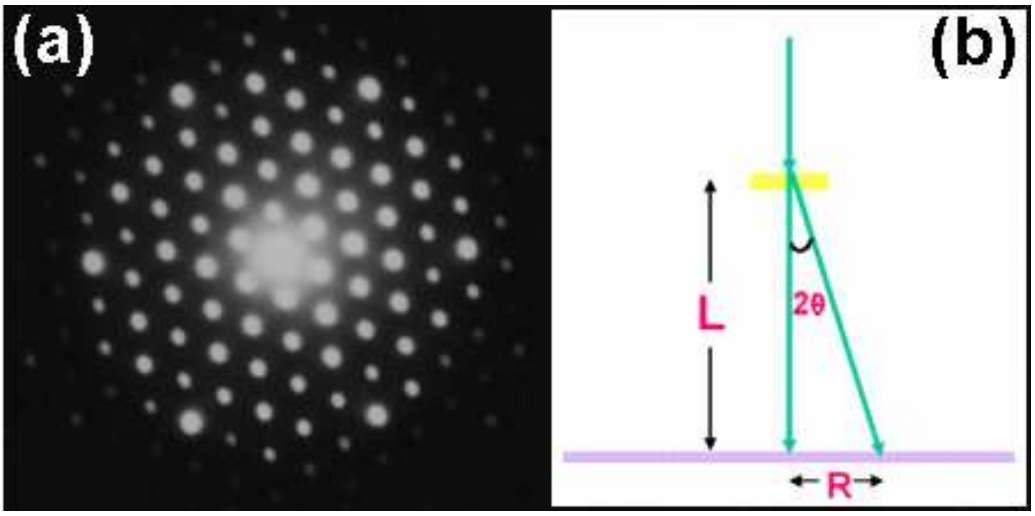

Figure 3.12 (a) A typical electron diffraction pattern for a crystalline specimen [16]. (b) The geometry of electron diffraction (note: no lenses have been shown, since they merely alter the effective camera length, L.)

Microdiffraction pattern (MDP) is another TEM technique that provides an effective means for the determination of crystal thickness as well as clear indications of the alignment of the axis of the beam with a crystal axis. It can be used as a very sensitive means for detecting changes of crystal orientation. Recent developments in combining MDP observations with high-resolution imaging have allowed more complete analysis of structures to become feasible [17]. Microdiffraction is a potential technique to determine the local structure characteristics at the atomic level. However, some problems still exist in both the experiment and the analyses, such as: (a) poor spatial resolution; (b) contamination; (c) difficulty in analyzing microdiffraction patterns taken under conditions of neither a completely coherent nor

completely incoherent illumination source. Improving these problems will make microdiffraction a more versatile tool to study microstructure [18]. MDP analysis in our study was performed in University of Oxford with a JEOL 3000 F TEM operating at 300 kV (L = 20 cm).

§ 3.3.6 Energy Dispersive X-ray Spectroscopy (EDX)

Energy dispersive X-ray spectroscopy (EDX or EDS) is an analytical tool predominantly used for chemical characterization. Being a type of spectroscopy, it relies on the investigation of a sample through interactions between light and matter, analyzing X-rays in this particular case. High energy electron beams (in an SEM or TEM) strike the material to be analysed, and X-rays are emitted. These X-rays can be detected by a SiLi detector, calibrated with respect to cobalt metal emission (6.925 keV), and then used to identify and analyze the elemental composition of the specimen surface. Its characterization capabilities are due in large part to the fundamental principle that each element of the Periodic Table has a unique electronic structure and, thus, a unique response to electromagnetic waves [19].

Essentially, an X-ray photon hits a diode in the detector producing a charge that is converted into a positive voltage pulse via a field effect transistor (FET). The pulse is subsequently converted by an analogue to digital converter, into a numerical value relative to the X-ray's incoming energy. The signal is then assigned to a particular energy channel and registered as a single count. Counts are compiled to produce an energy dispersive spectrum. The various emission lines associated with X-rays emitted from an atom are named after the shell of the initial vacancy, *i.e*. K, L, M, *etc*. A Greek letter subscript is used to indicate the shell of the electron that fills the gap. For example, K_α radiation refers to radiation resulting from a vacancy in the K shell being filled by an electron from the next highest shell. K_β denotes a K-shell vacancy filled by an electron from two shells above. There are some basic rules that apply for the order and energy of the X-rays:

1) For a given element, the lower line series has a higher energy, *i.e*. the energies of the K lines are greater than those of the L lines.

2) Within a line series, the higher atomic number elements emit higher energy X-rays. *i.e*. the oxygen K lines are higher in energy than carbon K lines.
3) The lower line series have simpler structures than the high line series, *i.e*. the K lines are simple, whilst the L and M lines get more complex and overlapping starts to occur.

EDX spectra can be acquired over short time-periods and be displayed almost simultaneously, providing a near instant visual representation of the chemical analysis. Qualitative analysis determines what elements are present in a sample by identification of the peaks in the spectrum, whilst quantitative analysis is used to derive the relative abundance of the elements from their corresponding peak intensities, either compared to other elements present in the spectrum or to standards.

For EDX, as a general rule of thumb, elements of $Z>11$ can be analysed if they are in a concentration of greater than 5 weight% with an accuracy of around ±3% if there are no significant peak overlaps. The analyst needs to think carefully about the sample (*i.e.* topography, porosity, *etc*), the lateral and depth resolution of the X-ray emission in relation to the sample microstructure, and the quoted accuracy of any computer generated results, before regarding EDX as a completely reliable black-box technique.

In this study, EDX analysis was used mainly to determine the bulk composition of the sample materials. In an SEM, a fixed accelerating voltage of 20 kV was used in order to obtain high signal intensity.

§ 3.3.7 X-ray Photoelectron Spectroscopy (XPS)

X-ray photoelectron spectroscopy (XPS) is a commonly used surface sensitive chemical analysis technique that operates under ultra-high-vacuum. When soft X-rays irradiate a sample surface, electrons will be ejected from valence and core levels of both surface and near surface atoms [20]. The kinetic energies of ejected photoelectrons are not only characteristic of the atoms from which they are emitted, but can also provide information on the chemical states of those atoms.

Figure 3.13 shows the basic process involved in XPS. It was found that during irradiation, electrons are only emitted from surface atoms when the energy of the X-rays is greater than a critical energy known as the *surface work function*, which is the energy required to excite an electron from its valence orbital to the continuum. For electrons emitted from lower lying orbitals, the binding energy of the electron also has to be overcome, reducing the kinetic energy of the emitted electron further [21].

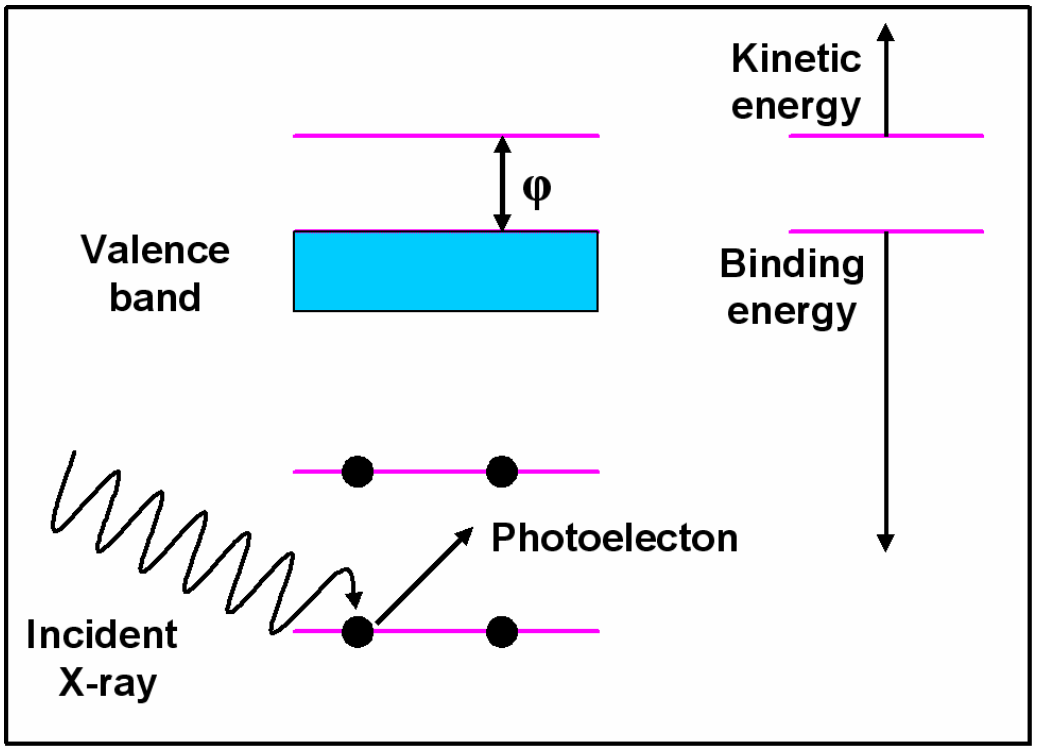

Figure 3.13 The mechanism of photoelectron emission in X-ray Photoelectron Spectroscopy.

Therefore, the kinetic energy of an ejected electron will be equal to the energy of the incident X-rays minus the work function, minus the binding energy of the electron. In XPS, the kinetic energy of ejected photoelectrons is measured by an analyser. The recorded kinetic energy is translated into a binding energy for the specific atomic orbital of an electron. Since each element has a unique set of energy

levels, each element also has a unique set of binding energies for electrons present in these levels.

The binding energy is described in the following equation:

$$E_B = h\upsilon - \varphi - E_K \quad (3.5)$$

Where E_B = electron binding energy/eV;

h = Planck's constant /eV.s;

υ= frequency of incident X-rays /s^{-1};

E_K = kinetic energy of electron /eV;

φ = surface work function /eV;

For a given element, slight variations in the location of corresponding photoelectron peaks result from small shifts in core energy levels, related to the oxidation state and bonding of the atoms. These peak variations are typically on the order of 1-5 eV, and can be detected by most XPS spectrometers if having energy resolutions of 0.1-0.2 eV.

XPS photoelectron peaks are named after the core level from which the electron has been emitted. For example, an electron from the iron 2*p* orbital gives a Fe *2p* peak. Ionisation of an *s* orbital leaves only a single energy ionic state, while *p*, *d* and *f* orbitals create two states of different energies, which appear in the spectra as two photoelectron peaks of different intensities.

The XPS technique analyses only the outer 1-10 nm of a sample because emitted photoelectrons lose kinetic energy as they travel through the sample. Only photoelectrons generated in the outermost layers of the sample have a short enough escape path to reach the detector.

In this study, XPS (Thermo VG Scientific) analysis was performed by Dr. Tom B Scott in the Interface Analysis Centre, University of Bristol. Photoelectrons generated by Al-K_α X-ray sources operating at 400 W (15 kV) having initial kinetic energies of up to 1486.6 eV, ensured an average depth for electron escape of ~1-10 nm. High resolution scans were acquired with 30 eV pass energy and 200 ms dwell times.

§ 3.3.8 Laser Raman Spectroscopy (LRS)

Raman spectroscopy is a spectroscopic technique used in condensed matter physics and chemistry to study vibrational, rotational, and other low-frequency modes in a system. It relies on inelastic scattering, or Raman scattering, of monochromatic light, usually from a laser in the visible, near infrared, or near ultraviolet range [22].

The Raman effect arises from inelastic scattering of photons by a solid, liquid, or gas. This effect is observed as a shift in the frequency of the scattered light relative to the excitation frequency. These energy transitions arise from molecular vibrations. Because these vibrations involve identifiable functional groups, when the energies of these transitions are plotted as a spectrum, they can be used to identify the molecule. The Raman effect was predicted by Smekal in 1923 [23], and later observed experimentally by Raman and Krishnan in 1928 [24].

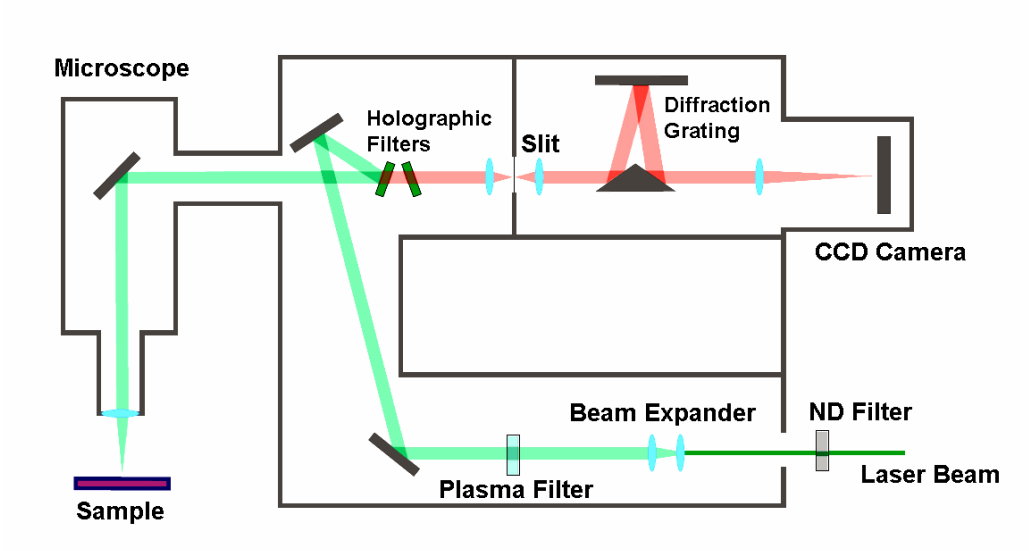

Figure 3.14 Schematic diagram of a Raman spectrometer.

Raman spectroscopy is commonly used in chemistry, since vibrational information is very specific for the chemical bonds in molecules. The main

advantages of Raman spectroscopy are its high information content, lack of sample preparation, compatibility with aqueous systems, and non-destructive nature.

The Renishaw RM2000 in the School of Chemistry is a multi-wavelength system with three different excitation sources: a 785 nm diode laser, the 514.5 nm line of an Ar^+ laser, and the 325 nm line of a He-Cd laser. The basic setup is outlined in Figure 3.14. In the present study, LRS was performed at 325 nm laser excitation, with a spectral resolution of 1 cm^{-1} (FWHM), determined by calibration using the output of a Ne lamp . This provides up to 20 mW on the sample in a spot diameter of ~ 1-20 mm. Each spectrum is typically an accumulation of 10 scans and is calibrated by the Si (100) peak at 520 cm^{-1}. A photo of the Renishaw Ramanscope used in this work is shown in Figure 3.15.

Figure 3.15 Photograph of Renishaw Raman spectrometer used in this study.

§ 3.3.9 Photoluminescence (PL)

Photoluminescence is a process in which a chemical compound absorbs photons (electromagnetic radiation), thus jumping to a higher electronic energy state, and then radiates photons, returning to a lower energy state [25]. Photo-excitation causes electrons within the material to move into permissible excited states. When these electrons return to their equilibrium states, the excess energy is released and may include the emission of light, or luminescence.

Photoluminescence (PL) spectroscopy [26] is mainly used as a diagnostic and development tool in semiconductor research, since it can provide information about the electronic structure and the emission mechanism of the material. Such studies are very important for the fabrication of electroluminescence devices such as light-emitting diodes and lasers.

In this work, room temperature PL spectra were recorded following excitation at 325 nm, with all the procedures the same as for the Raman spectrometry. The Renishaw Ramanscope (G92360) was operating with a Kimion K series HeCd laser which provided ~3 mW on the sample in a spot size of ~20 mm.

§ 3.3.10 Ultraviolet / Visible (UV / Vis) Absorption Spectroscopy

Ultraviolet-visible spectroscopy (UV / VIS) uses light in the visible and adjacent near ultraviolet (UV) ranges. At these wavelengths, molecules undergo electronic transitions [27]. In this technique, the light passes through the sample to be analysed, and some of the light is absorbed by the sample. Thus, the sample has to be thin enough such that some of the light is transmitted. Another factor is that the sample must be placed onto a supporting substrate, for example, quartz, that is transparent at the wavelengths of light used.

When visible or ultraviolet light is absorbed by the valence electrons of the material, these electrons are promoted from their ground states to higher energy excited states (Figure 3.16). The energies of the orbitals involved in electronic transitions have fixed values. The difference between the initial and final intensities

is recorded. When plotted into a spectrum as wavelength against absorbance, the absorbance is defined by using the Beer-Lambert law:

$$A = -\log_{10}\left(\frac{I}{I_0}\right) \tag{3.6}$$

where A is the measured absorbance, I_0 is the intensity of the incident light at a given wavelength, and I is the transmitted intensity, respectively. Most spectrometers display absorbance on the vertical axis, and the commonly observed range is from 0 (100% transmittance) to 2 (1% transmittance). The wavelength of maximum absorbance is a characteristic value, designated as λ_{max}.

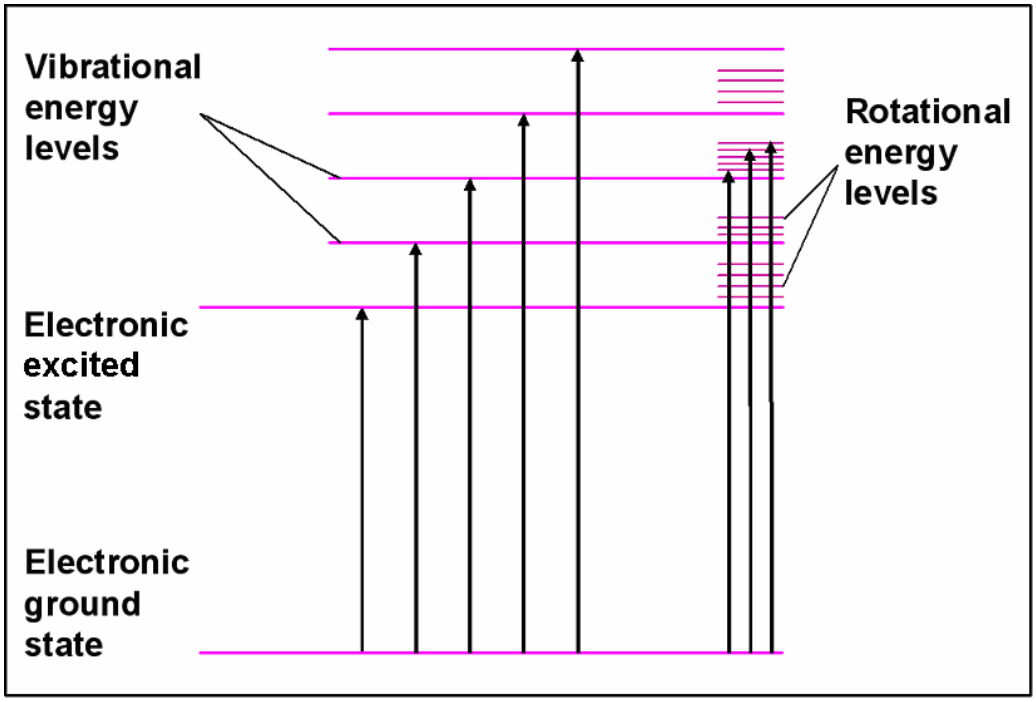

Figure 3.16 Illustration of the electronic transitions process during light absorption.

In a crystal, the band gap is defined as the minimum energy between the occupied valence band and empty conduction band. The two most common definitions are the E_{04} and the Tauc band gaps. The E_{04} band gap takes the value of

the photon energy for which the absorption coefficient equals 10^4. The Tauc gap is found by extrapolating the linear part of a plot of $(\alpha E)^{(1/2)}$ against the photon energy. The intercept of this line with the energy axis gives the value of the Tauc optical gap [28]. In this study, A UV-visible spectrophotometer (Perkin Elmer Lamda 11) was used to monitor the changes in absorbance of the ablated solution, allowing the Tauc optical band gaps to be calculated. After running the deionised water (or ammonia solution for carbon nitride) as background, a small amount of the collected liquid suspension (containing ablated products) was pipetted into a quartz cuvette with a 10 mm pass length without dilution. The cuvette was shaken slightly by hand to ensure the NPs were dispersed uniformly.

§ 3.3.11 Fourier Transform Infrared Spectroscopy (FTIR)

Fourier Transform Infrared spectroscopy (FTIR) is a technique based on the vibrations of the atoms within a molecule. An infrared (IR) spectrum is obtained by passing IR radiation through a sample and determining what fraction of the incident radiation is absorbed at a particular energy. The energy at which any peak in an absorption spectrum appears corresponds to the frequency of a vibration of a part of a sample molecule [29]. Moreover, chemical bonds in different environments will absorb varying intensities and at varying frequencies. Thus IR spectroscopy involves collecting absorption information and analyzing it in the form of a spectrum - the frequencies at which there are absorptions of IR radiation ('peaks' or 'signals') can be correlated directly to bonds within the compound in question. Because each interatomic bond may vibrate in several different motions (stretching or bending), individual bonds may absorb at more than one IR frequency. Stretching absorptions usually produce stronger peaks than bending, however the weaker bending absorptions can be useful in differentiating similar types of bonds (*e.g.* aromatic substitution).

The basic components of an FTIR spectrometer are shown schematically in Figure 3.17. The radiation emerging from the source is passed to the sample through an interferometer before reaching a detector. Upon amplification of the signal, in which high-frequency contributions have been eliminated by a filter, the data are

converted to a digital form by an analog-to-digital converter and then transferred to the computer for Fourier transformation to be carried out [30].

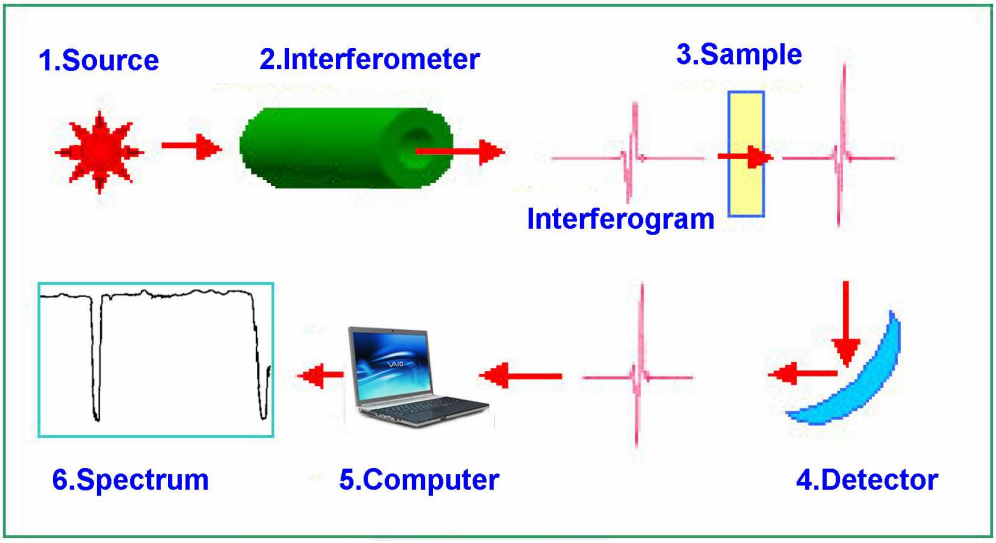

Figure 3.17 Schematic illustration of an FTIR system.

One of the great advantages of infrared spectroscopy is that virtually any sample in nearly any state can be studied. Liquids, solutions, pastes, powders, films, fibres, gases and surfaces can all be examined by a judicious choice of sampling technique.

FTIR spectroscopy (FTIR 8000, Perkin-Elmer) was carried out to study the potential existence of C-N, C=C and C≡N bonds during carbon nitride preparation. The FTIR sample handling is to grind finely a quantity of the sample with a specially purified salt (usually potassium bromide) to remove scattering effects from large crystals. This powder mixture is then crushed in a mechanical die press to form a translucent pellet through which the beam of the spectrometer can pass.

§ 3.3.12 Optical Emission Spectroscopy (OES)

During preparation using the LP-PLA method, light is emitted from excited species that are present within the ablation plume, which is clearly visible by eye. Light from different emitting species can be dispersed using a spectrometer, and the wavelengths of each peak assigned to different species using various references [31]. Thus, Optical Emission Spectroscopy (OES) gives a quick and easy way of identifying some of the species present in a plasma under different conditions.

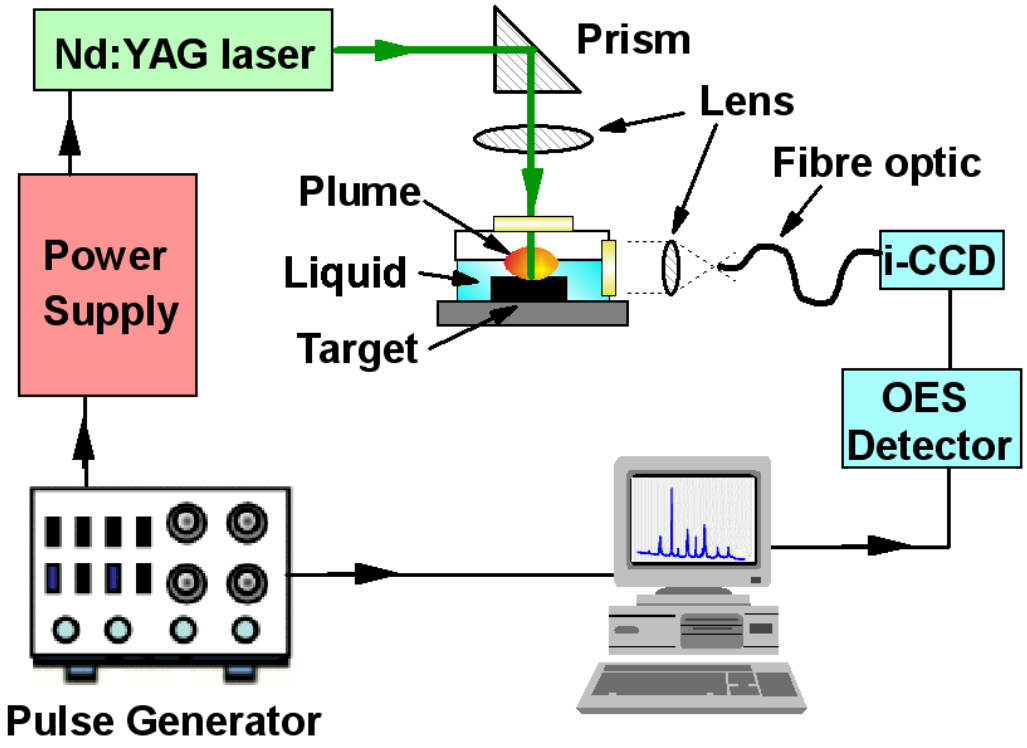

Figure 3.18 Experimental setup for LP-PLA and optical emission spectroscopy.

The optical emission accompanying the LP-PLA process was studied with the setup shown in Figure 3.18, viewed through a quartz window on the side of the cell, perpendicular to the laser direction. The emission was focused onto the entrance of a translatable single quartz fibre, the exit of which was adjacent to the entrance slit of a 0.32 m spectrometer. A narrow band-pass interference filter was placed in front of

the camera to block out the scattered light from the laser beam between 515-545 nm, but allow other wavelengths to pass through to the detector. Since the duration of the laser pulse and the emission lifetimes of the species within the plume were much shorter than the minimum exposure time for the detector (~0.019 s), it was not possible to record a series of time-resolved spectra showing the evolution of the emitting region. Therefore, the spectra were captured using a 1 μs time gate, delayed by 120 ns from the start of the laser excitation, and accumulated over 100 laser shots. This gave a time-averaged total emission spectrum covering the period of the whole ablation process.

Side-view images of the surface plasma emission were obtained by using an intensified CCD (i-CCD) connected to a computer with video capture software. The images were recorded by taking a continuous video during several laser pulses and analysing each frame of the video. A 656 nm filter (corresponding to the H Balmer emission line) was placed in front of the camera in order to obtain spatial information about the H atoms within the plume.

Bibliography

[1] Pearce S R J , Henley S J , Claeyssens F , May P W, Hallam K R , Smith J A, Rosser K N, *Diam. Relat. Maters.*, 2004, **13**, 661.

[2] Geusic J E, Marcos H M, Van Uitert L G, *Appl. Phys. Lett.*, 1964, **4**, 182.

[3] Niesen T P; De Guire M R, *J. Electroceram*. 2001, **6**, 169.

[4] Sounart T L; Liu J; Voigt J A; Hsu J W P; Spoerke E D; Tian Z; Jiang Y B, *Adv. Funct. Mater.* 2006, **16**, 335.

[5] Dick K A, Deppert K, Larsson M W, Martensson T, Seifert W, Wallenberg L R, Samuelson L, *Nat. Mater.*, 2004, **3**, 380.

[6] Ohlsson B J, Bjork M T, Magnusson M H, Deppert K, Samuelson L, Wallenberg L R, *Appl. Phys. Lett.*, 2001, **79**, 3335

[7] Borgström M, Deppert K, Samuelson L, Seifert W, *J. Cryst. Growth*, 2004, **260**, 18.

[8] Lu S N; Chung J, Ruoff R S, *Nanotechnology*, 2005, **16**, 1765.

[9] Skoog D A, West D M, Hollar F J, Crouch S R, *Fundamentals of Analytical Chemistry*, Thomson Brooks/Cole, USA, 2004.

[10] Filik J, *PhD thesis*, University of Bristol, 2006, pp. 77.

[11] Scott T B, *PhD thesis*, University of Bristol, 2005, pp. 53.

[12] Goldstein J I, Newbury D E, Echlin P, *Scanning Electron Microscopy and X-ray Microanalysis*, 2nd ed, Plenum Press, New York and London, 1992.

[13] Grundy P J, Jones G A, *Electron microscopy in the study of materials*, Edward Arnold Publishers Limited, 1976.

[14] http://en.wikipedia.org/wiki/Transmission_electron_microscopy

[15] http://en.wikipedia.org/wiki/Selected_area_diffraction

[16] http://www.matter.org.uk/diffraction/electron/electron_diffraction.htm

[17] Zhu J, Ye H Q, Cowley J M, *Ultramicroscopy*, 1985, **18**, 111.

[18] Zhu J, *J Electron Microscopy Technique*, 1987, **7**, 313.

[19] http://en.wikipedia.org/wiki/Energy-dispersive_X-ray_spectroscopy

[20] Moudler J F, Stickle W F, Sobol P E, Bomben K D, Chastain J (editor), *Handbook of X-ray photoelectron spectroscopy*, 2nd Edition, ISBN: 0962702625, Perkin Elmer Corporation, Minnesota, 1992.

[21] Wagner C D, Riggs W M, Davis L E, Mulder J F, Muilenburg G E (Editor), *Handbook of X-ray photoelectron* spectroscopy, 1st Edition, ISBN: 0962702621, Perkin Elmer Corporation, Minnesota, 1979.

[22] http://en.wikipedia.org/wiki/Raman_spectroscopy

[23] Smekal A, *Die Naturwissenschaften*, 1923, **43**, 873.

[24] Raman C V, Krishnan K S, *Nature*, 1928, **121**, 501.

[25] http://en.wikipedia.org/wiki/Photoluminescence

[26] Vij D R, *Luminescence of Solids*, Plenum Publishing Corporation,1998.

[27] http://en.wikipedia.org/wiki/UV/VIS_spectroscopy

[28] Tauc J, *Amorphous and liquid semiconductors*, Plenum, London and New York, 1974, pp. 171.

[29] Stuart B, *Modern Infrared Spectroscopy*, John Wiley & Sons Ltd, West Sussex, England, 1996, pp. 1.

[30] Stuart B, *Modern Infrared Spectroscopy*, John Wiley & Sons Ltd, West Sussex, England, 1996, pp. 24.

[31] Pearse R W B, Gaydon A G, *The Indentification of Molecular Spectra*, 4th edition, John Wiley & Sons, Inc, 1976.